ELSEVIER

Journal of Nuclear Materials 270 (1999) 376–381

journal of nuclear materials

Letter to the Editors

The crystal structure of oxides grown on Zr–20Nb alloy

O.T. Woo [a,*], Y.P. Lin [b]

[a] *AECL, Chalk River Laboratories, Chalk River, Ont., Canada K0J 1J0*
[b] *Ontario Hydro Technologies, 800 Kipling Avenue, Toronto, Ont., Canada M8Z 5S4*

Received 3 December 1997; accepted 12 March 1998

Abstract

Oxides that were grown on Zr–20Nb in water at 300°C for 3 d, or in air at 400°C for $\leqslant 2$ h were characterized by analytical electron microscopy. In both oxides, a similar microstructure was observed and similar electron diffraction patterns and high resolution lattice images were obtained. Analyses of the results showed that the crystal structure of the oxides was identical to that of an incommensurate modulated $Nb_2Zr_{x-2}O_{2x+1}$ phase, with $x \approx 10$. © 1999 Published by Elsevier Science B.V. All rights reserved.

Pressure tubes in CANDU nuclear reactors are made from Zr–2.5Nb. The typical pressure tube microstructure consists of elongated α-Zr platelets, 0.3 to 0.5 μm thick, surrounded by a thin layer of metastable β-Zr. The hcp α-Zr phase contains $\leqslant 1\%$ Nb in solution, while the bcc β-Zr phase contains ≈20% Nb in solution. Below ≈600°C, the metastable β-Zr decomposes to an equilibrium structure consisting of α-Zr and β-Nb ($\geqslant 80\%$ Nb) via $\beta\text{-Zr} \rightarrow \omega + \beta_{\text{Nb-enriched}} \rightarrow \alpha + \omega + \beta_{\text{Nb-enriched}} \rightarrow \alpha + \beta_{\text{Nb-enriched}} \rightarrow \alpha\text{-Zr} + \beta\text{-Nb}$ [1]. During service, an oxide will form on the pressure tube due to corrosion reaction with the coolant. Since the pressure tube microstructure changes with time in the reactor, the resultant oxide microstructure is expected to vary. The behaviour and relative importance of α-Zr and β-Zr phases are being studied using specially prepared Zr–Nb alloys with $\leqslant 20$ wt% Nb [2,3]. Oxides grown on Zr–1Nb (predominantly α-Zr) and on Zr–20Nb (β-Zr) to simulate those grown on a much finer scale on the α-Zr and β-Zr phases of pressure tube materials have been characterized by analytical electron microscopy (AEM) [3]. The oxide grown on Zr–1Nb was predominantly monoclinic ZrO_2, consistent with the crystal structure of oxides formed on α-Zr (e.g. [4–7]). The oxide on the Zr–20Nb was reported to have a nearly cubic crystal structure (tetragonal with a *c*/*a* ratio ≈1) during the initial stages of β-Zr decomposition [8]. This article is concerned with new electron diffraction results obtained from similar oxides on Zr–20Nb to refine the conclusions of Ref. [8]. The samples examined were part of an investigation to correlate hydrogen diffusion in Zr–Nb oxides with the oxide microstructure [3,9].

15 mm × 30 mm × 1 mm coupons of Zr–20Nb were vacuum-annealed at 850°C for 1 h and air-cooled. The resulting microstructure was single-phase β-Zr containing ≈20% Nb. Prior to corrosion testing, the coupons were abraded to 600 grit finish and then pickled in a mixture of 10% HF, 15% HNO_3, 30% H_2SO_4 and 45% H_2O. Some coupons were exposed to 300°C H_2O for 3 d in an autoclave, while others were oxidized in air at 400°C for $\leqslant 2$ h. The thickness of the oxides was typically 1–2 μm. Examination of the oxide by AEM was carried out in plan view. Thin slices cut from the coupon, with oxide on one side, were masked and then electropolished from the metal side to produce a web of oxide. The web was then ion-milled to electron transparency from the original free surface using 4 keV Ar^+ ions in a Gatan DuoMill with a cold-stage. This procedure made it possible to study the oxide from a region close to the metal/oxide interface. Characterization was carried out using a Philips CM30 or a JEOL 2010 AEM.

The microstructure of the oxide grown in 300°C water for 3 d, Fig. 1, consisted of predominantly oxide grown on single-phase β-Zr, with some areas having

---

[*] Corresponding author.

0022-3115/99/$ – see front matter © 1999 Published by Elsevier Science B.V. All rights reserved.
PII: S0022-3115(99)00024-0

hole-like appearances. The oxide grown in air at 400°C for $\leqslant 2$ h had a similar microstructure. High magnification micrographs of the oxide and the metal (in the thicker region of the foil), Fig. 2(a) and (b), revealed that the morphology and size of the hole-like features in the oxide were similar to those of the ω-phase particles. Thus the hole-like features were attributed to the removal of ω-phase particles during electropolishing.

Electron diffraction patterns showed the presence of strong and weak reflections. Analysis of the strong reflections indicated that the crystal structure of the oxide was loosely approximated by a cubic cell with a lattice parameter of ≈0.51 nm, consistent with [8]. Fig. 3(a) and (b) are examples of $\langle 1\ 0\ 0\rangle$-type selected-area diffraction patterns. A notable feature in these patterns was the presence of two, Fig. 3(a), or sometimes four, Fig. 3(b), satellite spots, depending on location in a given sample. The weak reflections were often most noticeable adjacent to the absent $\{1\ 0\ 0\}$-type reflections. Microdiffraction analyses, Fig. 4(a)–(c), revealed three variants contributing to the selected-area diffraction pattern shown in Fig. 3(a). These diffraction patterns were identified to be similar to those of a Zr–Nb–O solid solution phase, $Nb_2Zr_{x-2}O_{2x+1}$, $x = 7.1$–12.0, observed by Thompson, Withers and co-workers [10–12], briefly described as follows.

Originally thought to be part of a homologous series M_nO_{2n+1} $(x = 2n)$ [13,14], $Nb_2Zr_{x-2}O_{2x+1}$ is now considered to be a modulated phase, consisting of a superstructure based on modulation of orthorhombic metal and oxygen subcells which have slightly mismatched dimensions [10–12]. The mismatch in $Nb_2Zr_{x-2}O_{2x+1}$ occurs primarily in one direction of the crystal, such that x metal subcells are accommodated within $2x+1$ oxygen subcells; such a mismatch can be compared with a matching of two oxygen subcells per metal subcell in the fluorite structure of cubic ZrO_2. The mismatch in subcell dimensions can be regarded as the result of the need to accommodate more oxygen atoms due to the higher valence of Nb. Interaction of the two subcells results in a superstructure in which the positions of the metal and oxygen atoms deviate in a modulated

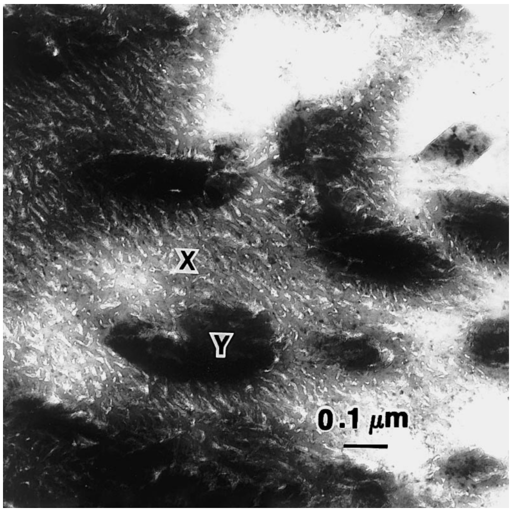

Fig. 1. Transmission electron micrograph of oxide on Zr–20Nb grown in 300°C water for 3 d, showing areas with hole-like appearances (*X*), and areas containing patches (*Y*) corresponding to regions of thick oxide.

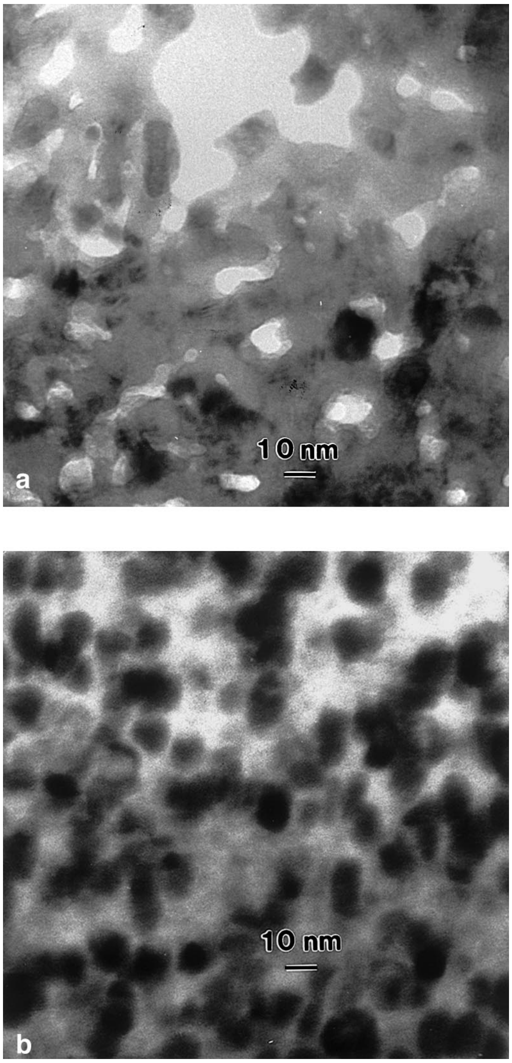

Fig. 2. High magnification micrographs of holey areas of oxide grown on Zr–20Nb in 300°C water for 3 d (a), and the metal (b), showing that the hole-like features were likely produced by the removal of ω-phase particles during electropolishing.

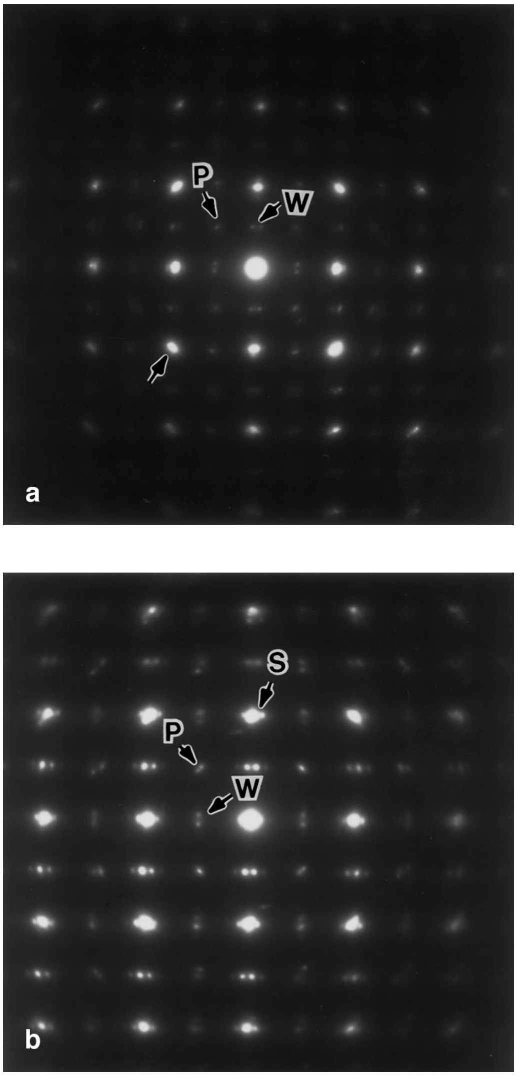

Fig. 3. Selected-area electron diffraction patterns of oxide on Zr–20Nb grown in 300°C water for 3 d (a), and oxide grown in 400°C for 1 h (b), showing strong (at S), and weak satellite (at W) reflections. Two or four satellite spots were observed in either oxide at various locations in each specimen. The splitting of the {1 1 0} type spots (at P) are due to the grains of one variant (see Fig. 4(a)) slightly misoriented to one another. Diffraction patterns in (a) and (b) were taken using different camera constants, thus the difference in size of the patterns.

manner from those in the respective average lattice; i.e. the modulation is structural rather than compositional ordering (of Nb). The modulation in effect enables two mismatched subcells to be accommodated. The resultant superstructure is x times larger than the metal subcell in the direction of the mismatch. Because x, being related to the Zr–Nb composition, is not a simple integer, the superstructure is incommensurate in nature. In electron diffraction patterns from such a superstructure, reflections associated with the superstructure appear as weak satellite reflections when located next to the strong reflections from the metal subcell. Interesting features of such a modulated superstructure description for $Nb_2Zr_{x-2}O_{2x+1}$ include the lack of distinct metal–oxygen distances and metal–atom coordination number varying between 7 and 8 for 0.26 nm limit of Zr–O bond [12]. In these respects, the structure of $Nb_2Zr_{x-2}O_{2x+1}$ is different from the cubic, tetragonal and monoclinic polymorphs of zirconia.

For the analysis of the present diffraction patterns, the superstructure is taken to have developed along the x-axis, in keeping with the crystal setting used by Thompson, Withers and co-workers [10–12]. The three variants contributing to the selected-area diffraction pattern shown in Fig. 3(a) can then be interpreted, with reference to the metal subcell, as respectively, a [1 0 0] pattern, Fig. 4(a); a [0 0 1] pattern, Fig. 4(b), with the satellite or weak reflections aligned parallel with the x-axis; and a second [0 0 1] pattern, Fig. 4(c), rotated 90° with respect to Fig. 4(b). The three variants correspond to superstructures developed along the normal to the oxide film and along two mutually perpendicular directions in the plane of the oxide film. Two of these variants were commonly observed, Fig. 5(a); they were imaged by dark field imaging using reflections (A and B) around the absent (0 1 0), Fig. 5(b) and (c). The presence of domains separated by anti-phase boundaries within the region of contrast in these dark field images is consistent with a low crystal symmetry.

In a previous work [8], a nearly cubic nature for this oxide was deduced based on Raman spectroscopy results, while the approximate (subcell) parameter of about 0.51 nm was obtained from microdiffraction patterns, the accuracy of which was compromised by the presence of weak satellite reflections. The c/a ratio was deduced from a doublet in X-ray diffraction. In the present work, the interpretation of selected area diffraction patterns in terms of different orientation variants described above allows the (metal) subcell parameters to be more accurately determined. The orthorhombic (metal) subcell parameters of the present oxide grown on Zr–20Nb, as measured from strong reflections in diffraction patterns such as Fig. 3(a) or (b), were $a \approx 0.513$ nm, $b \approx 0.499$ nm, and $c \approx 0.530$ nm. The accuracy of the measurements was $\approx 1\%$. For the present Zr–20Nb alloy, a value of 10.15 is expected for x based on a composition of 20% Nb. The measured subcell parameters are in remarkable accord with those for $x = 10$ reported by Thompson et al. [10].

High resolution electron micrographs taken at a diffraction condition close to that shown in Fig. 3 revealed fine and coarse fringes, Fig. 6, corresponding

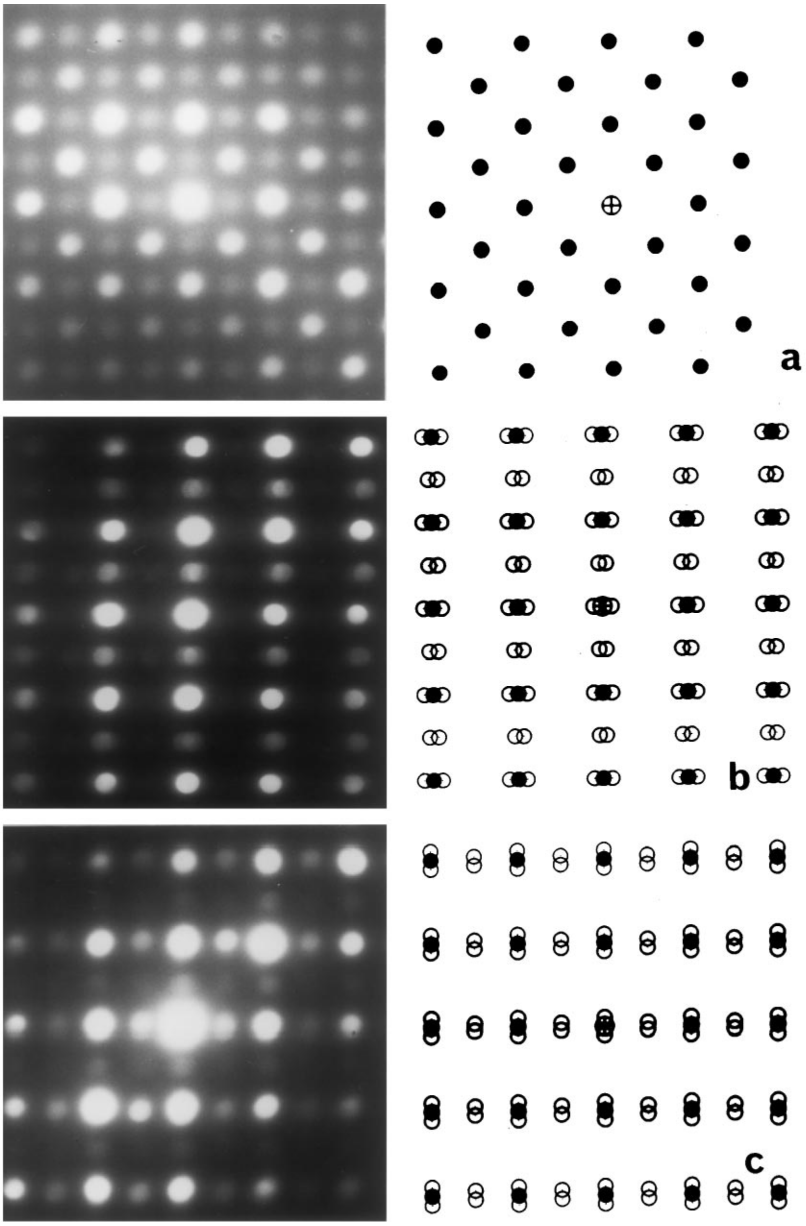

Fig. 4. Electron microdiffraction and simulated patterns, (a)–(c), showing the three variants contributing to the selected-area diffraction pattern shown in Fig. 3(a). Although (a) contains weak spots from interference of the variants in (b) and (c), the characteristic strong spot is the {1 1 0} type.

to spacings associated with metal subcell (2 0 0) and satellite reflections, respectively. The value of x can be estimated from the number of fine fringes per coarse fringe. The value obtained was 9.5 ± 0.3. Alternate estimates for x based on either spacing of satellite reflections in diffraction patterns or spacing of the coarse fringes were consistent with the above value. The estimated value of x is somewhat lower than the expected value of 10.15 for Zr–20Nb. The small discrepancy between the two values can be accounted for by the fact that the oxide regions examined were close to the metal/oxide interface, and therefore were oxidized from metal that would have undergone decomposition during corrosion. The

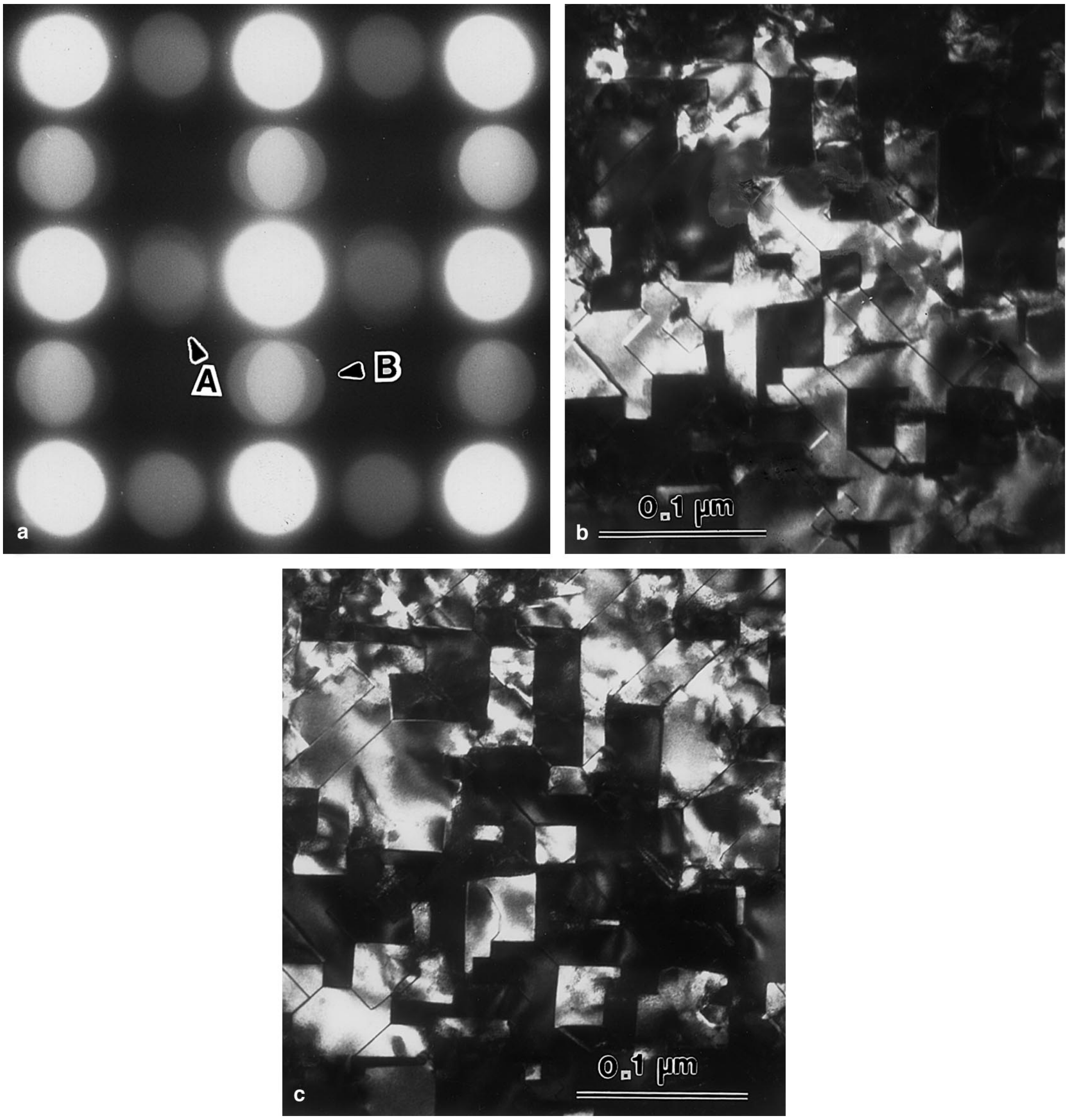

Fig. 5. (a) Microdiffraction pattern of the 400°C air-grown oxide showing two commonly observed variants. (b) and (c) Dark field micrographs taken with reflections A and B in (a) showing the two variants in complementary contrasts.

formation of the omega phase is expected to result in a more Nb-enriched β-Zr surrounding and hence a lower value of x.

Previous work [8] mostly based on Raman spectroscopy results had identified the initial oxide grown on Zr–20Nb as 'nearly cubic'. The identification originated from Raman spectra of the oxide which revealed two broad bands near 255 and 655 cm^{-1}, compared with the single broad band near 600 cm^{-1} for cubic zirconia and five bands from tetragonal zirconia. The present electron diffraction results however show that the initial oxide is more approximately described as an incommensurate modulated $Nb_2Zr_{x-2}O_{2x+1}$ phase, with $x \approx 10$.

In conclusion, the crystal structure of the initial oxide grown on single-phase Zr–20Nb is identical to that of an incommensurate modulated $Nb_2Zr_{x-2}O_{2x+1}$ phase, with $x \approx 10$.

Acknowledgements

This work was funded jointly by CANDU Owners Group, Work Project 35-3182, and by AECL CANDU

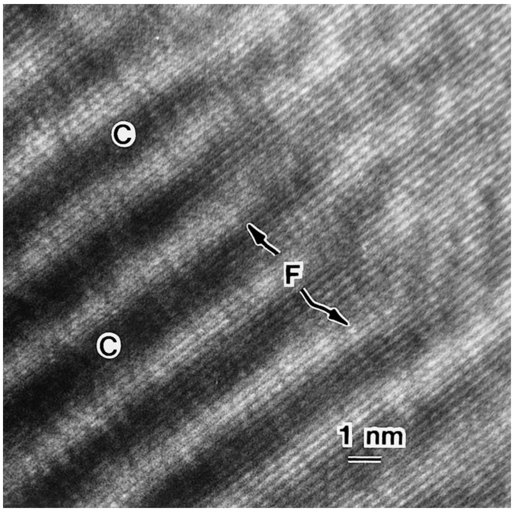

Fig. 6. High resolution micrograph showing coarse (C) and fine (F) fringes in the oxide. The fine fringes correspond to (2 0 0) spacings, while the coarse fringes are associated with the satellite reflections of the modulated incommensurate structure.

R&D Program, Project 501. We thank L.G. Laurin, A. Audet and V.C. Ling for experimental assistance, and R.L. Withers for valuable discussions.

References

[1] B.A. Cheadle, S.A. Aldridge, J. Nucl. Mater. 47 (1973) 255.
[2] V.F. Urbanic, to be published.
[3] V.F. Urbanic, P.K. Chan, D. Khatamian, O.T. Woo, in: A.M. Garde, E.R. Bradley (Eds.), Zirconium in the Nuclear Industry: International Symposium, ASTM STP 1245, American Society for Testing and Materials, Philadelphia, 1994, p. 116.
[4] C. Roy, G. David, J. Nucl. Mater. 37 (1970) 71.
[5] R.A. Ploc, J. Nucl. Mater. 110 (1982) 59.
[6] Y.P. Lin, O.T. Woo, D.J. Lockwood, Mater Res. Soc. Proc. 343 (1994) 487.
[7] X. Iltis, F. Lefebvre, C. Lemaignan, J. Nucl. Mater. 224 (1995) 109.
[8] O.T. Woo, D.J. Lockwood, Y.P. Lin, V.F. Urbanic, Mater. Res. Soc. Proc. 357 (1995) 219.
[9] D. Khatamian, Z. Physikal. Chem. 181 (1993) 435.
[10] J.G. Thompson, R.L. Withers, J. Sellar, P.L. Barlow, B.G. Hyde, J. Solid State Chem. 88 (1990) 465.
[11] R.L. Withers, J.G. Thompson, B.G. Hyde, Acta Crystallogr. B47 (1991) 166.
[12] K. Futterer, S. Schmid, J.G. Thompson, R.L. Withers, N. Ishizawa, S. Kishimoto, Acta Crystallogr. B51 (1995) 688.
[13] R.S. Roth, J.L. Warring, W.S. Browser, H.S. Parker, in: Solid State Chemistry, Proceedings of the Fifth Mat. Res. Symp., National Bureau of Standards Special Publication, 364, 1973, p. 183.
[14] J. Galy, R.S. Roth, J. Solid State Chem. 7 (1973) 277.